Materials Horizons

Estimating the lower-limit of fracture toughness from ideal-strength calculations

Journal:	*Materials Horizons*
Manuscript ID	MH-COM-11-2021-001831
Article Type:	Communication
Date Submitted by the Author:	11-Nov-2021

Complete List of Authors:	Borgsmiller, Leah; Northwestern University, Materials Science and Engineering Agne, Matthias; Northwestern University, Materials Science and Engineering Male, James; Northwestern University, Materials Science and Engineering Anand, Shashwat; Northwestern University, Materials Science and Engineering Li, Guodong; Wuhan University of Technology, Morozov, Sergey ; South Ural State University, Physics of Nanoscale systems; Snyder, G.; Northwestern University, Materials Science

New Concepts Statement

Fracture toughness is an incredibly important material property for engineering design of practical materials. However, the fracture toughnesses of many materials, particularly electronic materials, is not always well documented. This work introduces a new method for estimating the lower limit of fracture toughness for a variety of different materials using ideal strength calculations. We call this method the Integral Stress-Displacement Method. We show good agreement between experiment and this method, particularly for single crystal experiments. This work is distinct from other methods in that it aims to capture thermodynamically irreversible processes. In this study we provide a link between computed ideal stress-strain curves and observed fracture behavior. As this method is an estimation of the lower bound of fracture toughness, it can be used as an engineering benchmark to provide approximations for fracture toughness values for materials without well studied fracture behavior. This model can also be used as a starting point for more advanced models of material fracture and is predictive of single crystal fracture toughness values.

Estimating the lower-limit of fracture toughness from ideal-strength calculations

Leah Borgsmiller[1,†], Matthias T. Agne[1,†,*], James P. Male[1], Shashwat Anand[1], Guodong Li[2,3], Sergey I. Morozov[4], and G. Jeffrey Snyder[1,*]

[1]Northwestern University, Materials Science and Engineering, Evanston, IL 60208
[2]Wuhan University of Technology, State Key Laboratory of Advanced Technology for Materials Synthesis and Processing, Wuhan 430070, China.
[3]Wuhan University of Technology, Hubei Key Laboratory of Theory and Application of Advanced Materials Mechanics, School of Science, Wuhan, 430070, China
[4]South Ural State University,Department of Physics of Nanoscale Systems, Chelyabinsk 454080, Russia
[*]mt.agne.matsci@gmail.com, jeffsnyder@northwestern.edu
[†]contributed equally

ABSTRACT

Fracture mechanics is a fundamental topic to materials science. Fracture toughness, in particular, is a material property of great technological importance for device design. The relatively low fracture toughness of many semiconductor materials, including electronic and energy materials, handicaps their use in applications involving large external stresses. Here, it is shown that quantum-mechanical density functional theory calculations of ideal strength, in conjunction with an integral stress-displacement method, can be used to estimate the fracture energy needed to calculate fracture toughness. Using the fracture energy associated with the weakest crystallographic direction provides an estimation for the lower-limit of the fracture toughness of a material. The lower-limit values are in good agreement with experimental single crystal measurements across several orders-of-magnitude of fracture toughness. Furthermore, the proposed methodology is useful for benchmarking experimental measurements of fracture toughness in polycrystalline materials and can serve as a starting point for the construction of more detailed fracture models and the computational design of new materials and devices.

1 Introduction

The resilience of a material to fracture is defined in part by its fracture toughness, which describes the conditions for crack growth to occur. Since even ambient stresses present in everyday devices can be problematic for some materials, fracture toughness is an important engineering design metric. In particular, the utility of semiconductor materials for applications having applied stresses often requires clever engineering solutions. Thermal and vibrational stresses are often present in electronic [1, 2] and energy materials [3, 4] (including those used for efficient gas turbines [5]) during operation. Additionally, new, tough materials are desired for modern applications, such as internet-of-things devices [6]. However, fracture toughness measurements can be difficult and complicated, especially in brittle semiconducting materials. As such, reported fracture toughness values can be sparse, and well-defined methods to benchmark fracture toughness improvements are lacking. To this end, establishing a lower-limit for fracture toughness has wide-spread engineering utility.

The mechanical failure of materials by fracture (or rupture) is an inevitable result of the finite strength of atomic bonds. Although bonding is the fundamental material property that determines fracture conditions, defects (e.g. cracks) are often the primary focus since they serve to amplify local stresses well beyond the nominal external stress applied to the material. Griffith [7] was the first to recognize that material properties (i.e. bonding) and system properties (i.e. stress state and defect geometry) were connected through a thermodynamic criteria for fracture. Later, Irwin [8] and Orowan [9, 10] expounded upon Griffith's work and defined fracture toughness, K, as the inherent material property which determines fracture conditions. For plane strain conditions, the mode I (tensile force acting to open the crack) fracture toughness, K_{Ic}, is given by

$$K_{\mathrm{Ic}}^2 = G_{\mathrm{Ic}} E/(1-\nu^2) = \phi \sigma_{\mathrm{f}}^2 a_{\mathrm{c}} \tag{1}$$

where E and ν are the Young's modulus and Poisson's ratio for an isotropic material, G_{Ic} is the work of fracture per unit area, σ_{f} is the nominal stress needed for fracture to occur in a material with critical crack length, a_{c}, and ϕ is a numeric factor depending on the geometry of the crack. For brittle materials having an elliptical crack, Griffith found that $\phi = \pi$ and $G_{\mathrm{Ic}} = 2\gamma_{\mathrm{s}}$, where γ_{s} is the surface energy and the factor of 2 arises from the 2 surfaces created. Orowan and Irwin generalized the Griffith result to include ductile fracture, but the form of Eq. 1 is retained. In the general sense, G_{Ic} is the energy per unit area needed to create additional surfaces.

For mode II (shear force in the plane of the crack, parallel to the crack direction) in the plane strain condition, Rice [11]

derived the fracture toughness K_{IIc} as

$$K_{IIc}^2 = 2G_{IIc}\mu/(1-\nu) \quad (2)$$

where μ is the shear modulus and G_{IIc} describes the energy per unit area to create additional surfaces through shear. Rice calls this the unstable stacking energy corresponding to the nucleation of a full dislocation.

Fracture toughness is typically assessed by finding the critical crack length for a given applied stress. This is largely because the fracture energy, G, is difficult to obtain experimentally. Computational methods, however, can calculate energies directly.

The "surface energy" relevant to fracture is the energy required to break atomic bonds and form a new surface (i.e. $G/2$). This is not necessarily the same surface energy as γ_s, which describes the excess energy due to the dangling bonds of a relaxed surface. Griffith made the approximation that $G = 2\gamma_s$ for brittle materials. This approximation is valid when surfaces are made via thermodynamically reversible processes, which is not necessarily the case due to the complexity of fracture [12, 13] (e.g. plasticity). Nevertheless, there are straightforward computational methods (e.g. the Boettger method [14, 15] or other "slab methods") to calculate γ_s. Several models, with varying degrees of complexity, estimate fracture toughness using Griffith's approximation and γ_s calculations [16, 17, 18, 19, 20].

Herein, we do not use the Griffith approximation, but introduce the integral stress-displacement method as a way to estimate G. The integral under any stress-strain curve is the total mechanical energy stored in the material per unit volume (i.e. energy density). When the material is strained to failure, integrating up to the failure strain describes how much work was done to the material to fracture it. This is often called toughness [21]. Alternatively, the integral of a stress-displacement curve taken up to the point of fracture has units of energy per unit area and describes the energy required to create new surfaces when the material fractures. Thus, the fracture energy G, a material property defined by atomic bonding, can be estimated from atomic scale stress-displacement curves obtained by computational methods (Fig. 1).

Specifically, we show that the fracture energies G_{Ic} and G_{IIc} can be estimated from the integral stress-displacement method using the ideal stress-displacement curves obtained by density functional theory (DFT) calculations. The G estimation can then be used to calculate a fracture toughness value (Eqs. 1 and 2). By using the ideal strength of the weakest crystallographic direction to estimate G, our method provides a lower-limit value of fracture toughness. The values of fracture toughness found here are in good agreement with the lowest values obtained in single crystal experiments. Given the numerous complexities of fracture in real materials, this methodology provides a relatively simple benchmark value of fracture toughness and a starting point for more detailed models and analyses. Estimating the lower-limit of fracture toughness is highly useful for engineering design, both for safety and device lifetimes – especially for materials where experimental fracture toughness data is not readily available.

2 Methods

Stress and crack length can be measured experimentally to calculate fracture toughness (e.g. Eq. 1), but experimental determination of the fracture energy G is not directly possible. However, atomistic computational methods allow for reasonable estimations of G quite readily since they can investigate bonding directly. In short, by probing bond strengths directly, computational techniques can be used for comparative studies of the magnitude of fracture toughness and the estimation of a lower limit.

Here, the important idea is that fracture energy is estimated from the energy contained by the atomic bonds at the point of failure. That is, the integral of the stress–displacement ($\sigma - l$) curve from the initial equilibrium bond position up to the point of failure (Fig. 1),

$$G = \int_{\text{equilibrium}}^{\text{failure}} \sigma \cdot dl. \quad (3)$$

Since the stress for a given displacement is easily obtained by computational methods, the fracture energy is also readily calculated. This expression is completely general and can be applied to obtain fracture energies along any displacement direction for any atomic structure of interest, and is named here as the integral stress-displacement method. In this work, we utilized the weakest crystallographic direction of perfect crystals to obtain a lower limit estimate of fracture energy. Obtaining these estimates of G computationally allows for the calculation of fracture toughness values for a wide variety of crystalline materials, which can subsequently be used for engineering design.

Ideal strength calculations were undertaken for TiC and TiN. TiC and TiN were selected because their mechanical properties are of interest for practical applications and their fracture behavior is relatively well characterized experimentally [22, 23, 24, 25] and computationally [26]. All density functional theory (DFT) calculations were performed by the Vienna ab initio Simulation Package (VASP). The Perdew-Burke-Ernzerhof (PBE) exchange-correlation functional with the projector augmented wave (PAW) method was used to account for the core-valence interactions [27, 28, 29]. A plane wave cutoff energy of 500 eV gave good convergence for the total energies. The convergence criteria were set to 1×10^{-6} eV energy difference for solving the electronic wave function and 1×10^{-2} eV/Å force for geometry optimization. All calculations used the Γ-centered Monkhorst-Pack scheme with a fine resolution of $2\pi \times 1/40\text{Å}^{-1}$ in the k-point reciprocal space sampling. The detailed quasi-static mechanical loading setup of TiC and TiN is similar to our previous calculations on thermoelectric materials [30, 31, 32].

In order to obtain the fracture energy, G, the integral of the stress-displacement curve is needed. While the ideal stress-strain curves for TiC and TiN are reported here, the ideal

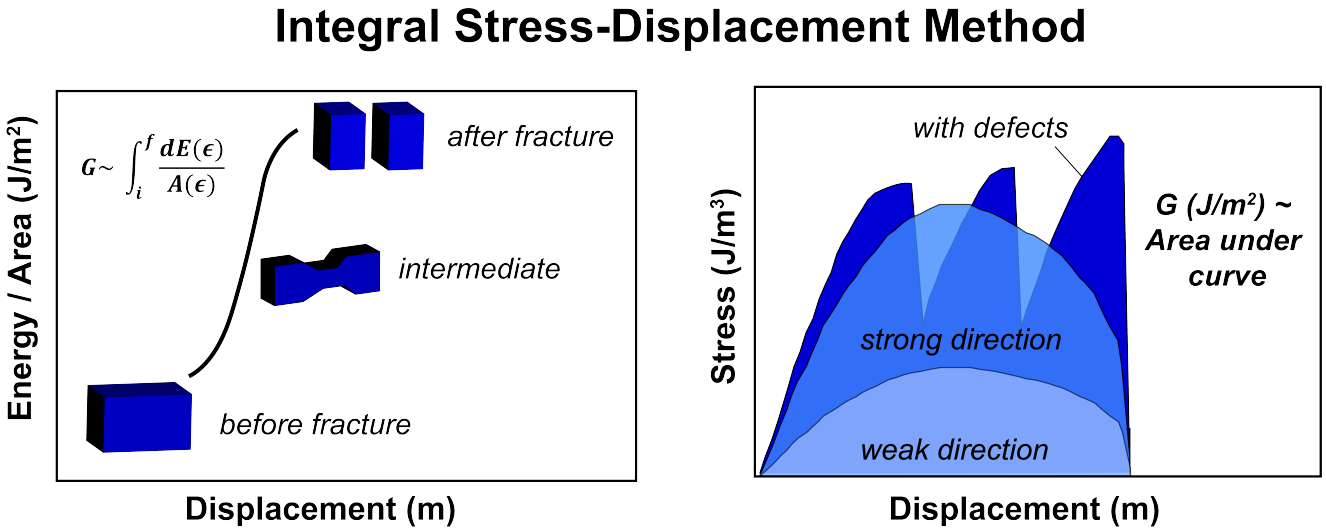

Figure 1. The integral stress-displacement method of determining the fracture energy, G. The physics of fracture is captured by the continuous deformation of the atomic structure in the computational simulation (left). The work required to create two new surfaces is found by integrating the stress-displacement curve (right). The stress-displacement curve is expected to be different for different crystallographic directions within a material (illustrated as 'strong direction' and 'weak direction' in figure), and can be impacted by the presence of defects, such as twins, to the crystallographic structure. These defect structures may or may not increase fracture energy. For this work, we integrated under the curve for the weakest crystallographic direction, probing the lower-limit of fracture toughness.

stress-strain curves for the other compounds can be found elsewhere [33, 34, 35, 36, 31, 32, 37, 30, 38, 39, 40, 41, 42]. A detailed procedure for converting the stress-strain curve to a stress-displacement curve can be found in Supplemental Note 1. In short, knowledge of the unit cell was utilized for each material in order to convert strain to absolute displacement. Then, numerical integration was performed in MATLAB using interpolant fitting between data points. In some cases, linear regressions were used to approximate the stress-displacement relation at the largest displacements. This procedure is unlikely to affect the estimate of G by more than a few percent. As fracture toughness goes as $\sqrt{G}$, small uncertainties in G have negligible consequences for the conclusions drawn from the resulting calculation of fracture toughness. The stress-displacement curves used for integration in this study can be found in the Supplemental Information. The values for unit cell parameters, modulii, Poisson's ratio and estimated fracture toughness for all of the materials in this study are compiled in Table S1.

In principle, any number of computational methods, for example those based on density functional theory (DFT) or molecular dynamics (MD), could be used [43, 44]. Some different techniques for calculating ideal stress-strain curves have been discussed before [45, 46], but small differences in the estimation of G are not expected to inhibit the practicality of using a consistent computational methodology to provide engineering guidelines for fracture toughness.

3 Results

Ideal strength calculations were undertaken for TiC and TiN using density functional theory (DFT) methods. In both cases, shear stresses were applied to TiC and TiN along the (100)/<011> slip system resulting in mode II fracture. These stress-strain curves are shown in Fig. 2a. The ideal strength (i.e. the maximum stress that the material can reach) is 32.5 GPa for TiC and 29.8 GPa for TiN under these loading conditions. The bond lengths demonstrating the response of bonds to shear strain are shown in Fig. 2b. The discontinuity in bond length at the point of maximum strain is indicative of fracture. Crystallographically, the structures of TiC and TiN just before fracture show the large shear deformation (Fig. 2c). The corresponding structures at the point of failure are also shown in Fig. 2c. We note that these DFT calculations likely only approximate fracture behavior in that they capture the energetics of material deformation leading up to a distinct structural change (i.e. bond breaking). For example, in these idealized simulations there may be energetic competition between fracture and structural phase transformations, but the energy landscape is expected to be close enough to provide a realistic estimate of the fracture energy regardless.

Using the integral stress-displacement method (Fig.1) along the weakest crystallographic direction, we estimated the fracture energy (per unit area) G from both our TiC and TiN calculations and from several previously reported ideal strength calculations [33, 34, 35, 36, 31, 32, 37, 30, 38, 39, 40, 41, 42] (stress–displacement curves shown in Figs. S1-21). The estimate of G and bulk elastic properties found from DFT

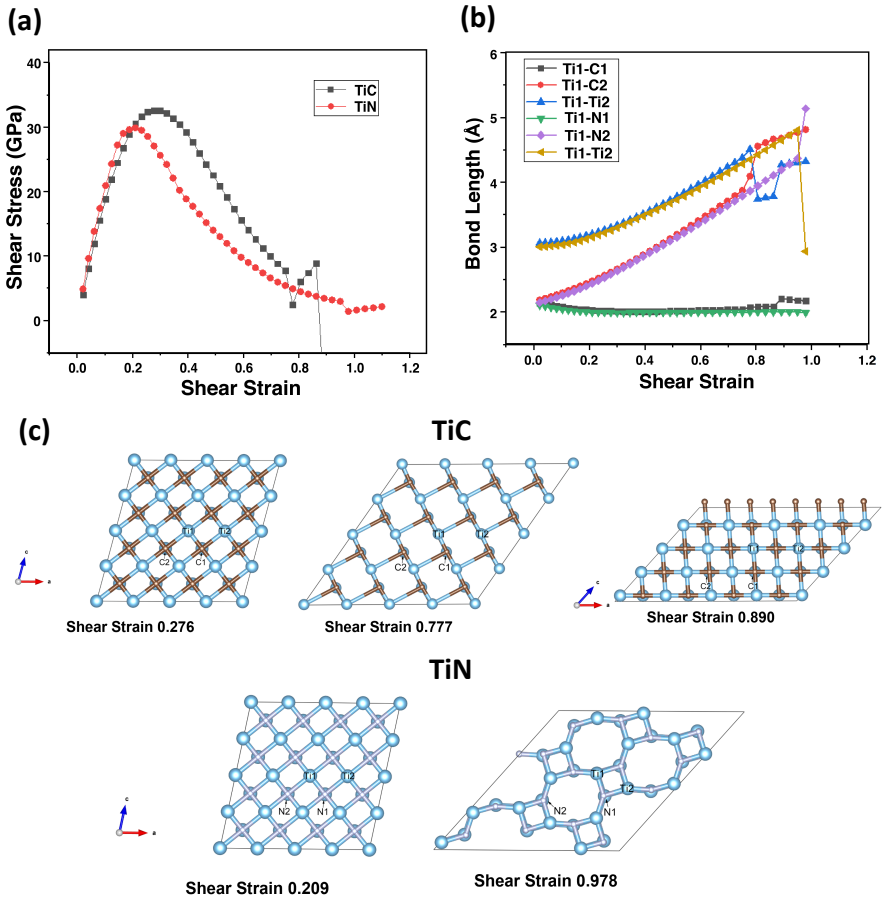

Figure 2. (a) Ideal stress-strain curves for TiC and TiN under shear conditions. (b) Bond length against shear strain of TiC and TiN. (c) Lattice deformation in TiC and TiN as a result of applied shear stress right before failure and at the point of failure.

were used in Eq. 1 or 2 (depending on the mode of fracture) to calculate lower-limit fracture toughness values. Comparisons to experimental results are tabulated in Table S2. Surface energies of relaxed structures were also calculated for several materials and used to provide an additional estimation of G as a point of comparison (Supplemental Note 2).

4 Discussion

Fracture toughness is an important limiting factor for device implementation and lifetime. The desire for computational materials design necessarily includes having estimates of fracture toughness, K, that can be used for engineering purposes. Herein, K is calculated from the fracture energy per unit area, G, estimated from ideal strength calculations. The integral stress-displacement method (Eq. 3 and Fig. 1) was applied to the idealized case of fracture occurring on the weakest crystallographic plane in order to consider the lower-limit of fracture toughness in each material.

The physics of fracture on the atomic scale is the breaking of and/or rearrangement of atomic bonds. While the loading geometries and distribution of internal stresses within bulk materials is vastly more complicated, computational materials techniques (e.g. DFT or molecular dynamics) are well-suited to investigate specified loading conditions on local atomic structures. In particular, the "ideal" strength of crystalline solids can be investigated, which is found from the stress-strain behavior of a defect-free "perfect" crystal. The magnitude of the ideal strength depends on the loading geometry and crystallographic direction. A pure tensile stress tends to induce cleavage between atomic planes. Shear stress tends to induce the formation of dislocations. Generally, ideal shear strengths are lower than ideal tensile strengths, reflecting the experimental evidence that dislocations govern deformation in many crystals [12, 13]. Furthermore, for a particular applied stress, certain crystallographic directions are stronger than others. "Cleavage planes" are typically planes of high atomic density that are the first to fracture in brittle materials. Ductile fracture has additional complexities such as void nucleation and coalescence [62]. Molecular dynamics calculations may be more appropriate than DFT to probe fracture behavior at this length scale, however the formalism developed here (Eq. 3) can still be used [63].

In general, crack propagation will depend on the local

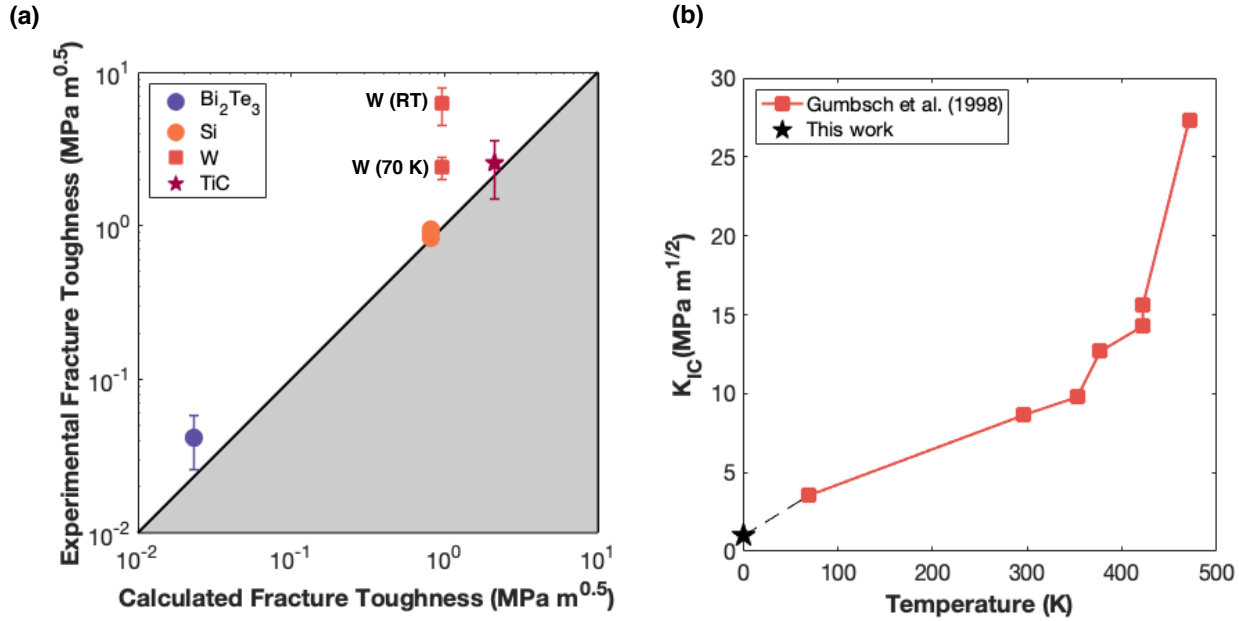

Figure 3. (a) Comparison between fracture toughness values measured experimentally for single crystals [23, 47, 48, 49, 50] and those calculated using fracture energies estimated from the integral stress-displacement method. This calculation is an estimate of the experimental fracture toughness in bulk materials using the idealized case where fracture occurs in the weakest crystallographic direction and without consideration of any additional toughening mechanisms. Both mode I and mode II fracture toughness calculations are plotted (see Table S1). This plot demonstrates good agreement between single crystal experiments and calculation for all materials except for tungsten due to the temperature dependent fracture behavior in tungsten shown in panel b. (b) Temperature dependent behavior of the fracture toughness of single crystal tungsten[50]. Extending the curve from Gumbsch et al.[50] to 0 K agrees well with our 0 K DFT calculation using the integral stress-displacement method.

stress state relative to crystal orientation near the crack tip. Consequently, the weakest crystallographic plane may not always be the preferential crack growth direction. This is particularly relevant for bulk polycrystalline materials where the relative orientation of adjacent grains can influence crack propagation. Here, fracture toughness is calculated using the fracture energy G estimated from the weakest crystallographic direction in either shear and/or tensile loading. This is representative of the idealized case of fracture occurring along the weakest crystallographic plane, without crack deflection or other toughening mechanisms present. This calculation of K is thus expected to be a lower limit. While experimental results for non-defective single crystal samples loaded in a similar geometry are expected to be comparable in magnitude to the calculated values, the calculation only provides a lower-limit benchmark value for the experimental characterization of fracture toughness in polycrystalline materials.

Agreement with single crystal experiments is demonstrated in Figure 3. Here, our lower-limit fracture toughness calculation appears to be a good predictor of the magnitude of the experimental fracture toughness values for TiC, Si and Bi_2Te_3. The close agreement with single crystal data is not surprising since the DFT calculations are representative of 0 K conditions for a perfect single crystal. Toughening mechanisms (e.g. defects) introduced at higher temperatures or polycrystalline conditions, which typically increase the effective value of G, are not taken into account and thus we would expect our calculated fracture toughness values to be at the lower bound of experimental work.

TiC has well-studied mechanical properties due to its high melting point and high hardness making it valuable in high temperature applications such as components for jet engines and rocket nozzles [64]. The single crystal fracture toughness (as determined by a Vickers indentation method) is reported to be $\sim$1.5 MPa $\sqrt{\text{m}}$ for a crack aligned in the [100] direction on the (001) plane, but can be as high as $\sim$3.6 MPa $\sqrt{\text{m}}$ for other crystallographic orientations [23]. From the (100)/<001> shear result (Fig.2) the calculated fracture toughness is $\sim$2.1 MPa $\sqrt{\text{m}}$, which is in good agreement with these experiments given the uncertainty of the experimental method ($\sim$ 30%[23]) and the simple approach to estimating fracture energy undertaken herein. It should also be noted that the

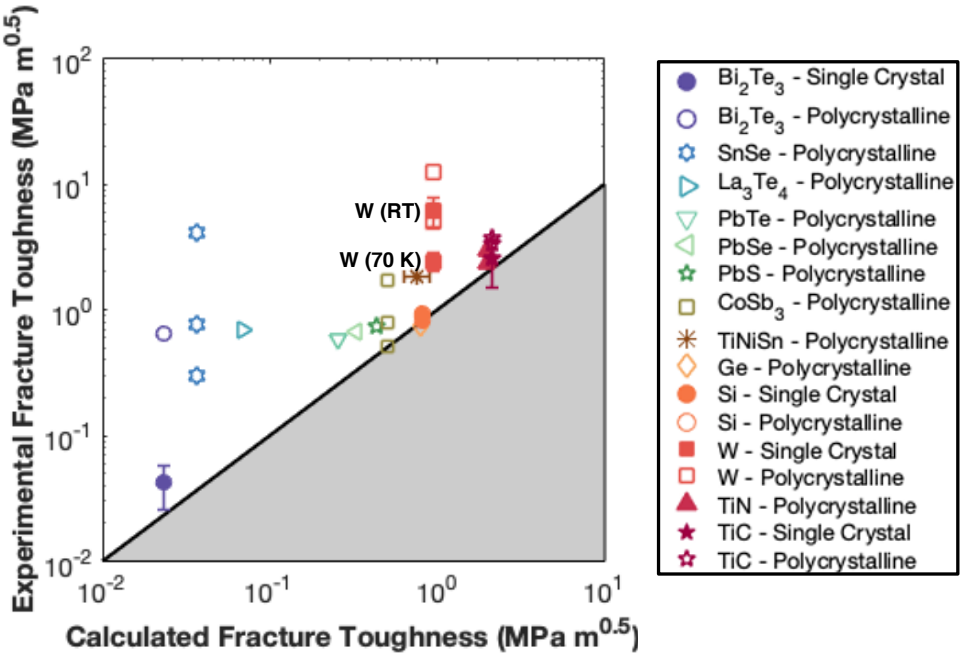

Figure 4. Comparison of fracture toughness values measured experimentally for both polycrystalline and single crystalline samples [47, 51, 52, 53, 54, 31, 55, 56, 57, 22, 23, 58, 59, 60, 48, 49, 50, 24, 25, 61] to those calculated using fracture energies estimated from the integral stress-displacement method. All markers that lie above the black diagonal line have higher experimental fracture toughness values than calculated fracture toughness values. Thus, while this approach captures the magnitude of single crystal results very well (as seen in Figure 3), these calculations serve as a lower bound for polycrystalline fracture toughness.

loading conditions realized experimentally may not be strictly mode I or II, but can have mixed character. As illustrated in Fig. 1, the area under the curve, G, can vary between the weak and strong crystallographic directions. Thus, if a material does not fracture along the weakest direction it is expected that the fracture toughness would be greater.

The calculated fracture toughness of Si also showed good agreement with single crystal experiments [48, 49]. Here, our value of $K = 0.82$ is directly comparable to the values $K = 0.83$[48], 0.95[48], and 0.91[49] MPa $\sqrt{\text{m}}$ (determined by different methods) for cracks propagating in the $\{111\}$ and $\{110\}$ cleavage planes.

For the layered material Bi_2Te_3, which is relevant for thermoelectric applications near room temperature [65], our calculated fracture toughness (~ 0.02 MPa $\sqrt{\text{m}}$) corresponds to the lower bound of the experimental value for a single crystal (0.042 ± 0.016 MPa $\sqrt{\text{m}}$ [47]).

For tungsten single crystals it was initially surprising that the calculated fracture toughness served as a lower-limit estimation of experimental values rather than a quantitative prediction. However, this apparent discrepancy illustrates that our methodology can be a starting point for more complex analysis. Crucially, the DFT calculation is representative of the material behavior at 0 K. It has been shown experimentally that tungsten undergoes a ductile to brittle transition causing the fracture toughness to decrease substantially with decreasing temperature [50, 66]. This phenomena is fairly common in other body-centered cubic (BCC) refractory metals[67], whereas other structures can be less sensitive to changes in temperature. Our estimation for the fracture toughness of single crystal W is in better agreement with low temperature measurements extrapolated to 0 K (see Figure 3b). Thus, this method of estimating the lower-limit of fracture toughness is likely to only be quantitatively predictive for single crystals under certain conditions.

Given the good agreement with single crystal experiments (Figure 3), we also demonstrate that our method provides a lower-limit estimation for the fracture toughness of polycrystalline materials (Figure 4). Because fracture toughness studies on polycrystalline materials are more common, we were able to draw a larger comparison than in the single crystal case. Even though experimental fracture toughness values can vary drastically for the same material, the estimated K provides a realistic lower bound for fracture toughness. Exper-

imental values much larger than the estimated lower-limit are likely due to additional toughening mechanisms not captured by the present method, such as the effects of polycrystallinity [68]. For example, polycrystalline experiments of fracture toughness for TiC report values around 3.6 MPa $\sqrt{m}$ [23, 22]. Further efforts using alloying and introducing nanostructures have been found to increase the fracture toughness of TiC to $\sim$7 MPa $\sqrt{m}$ [64, 69]. Additionally, discrepancies between experimental polycrystalline fracture toughness values for the same material can be attributed to other sample characteristics such as the grain size [70], or shortcomings in the measurement methods themselves (e.g. the unreliability of the Vickers indentation method for absolute values of fracture toughness [71]).

Thin film TiN is incredibly useful for microelectronics [72, 73, 74], corrosion protective coatings [75, 25], and energy material applications [76, 77, 78]. These applications often include high stress states that necessitate an understanding of mechanical properties, including fracture behavior. Thin film TiN has been reported experimentally to have a fracture toughness of about 2.3-2.9 MPa $\sqrt{m}$ [25, 24], in good agreement with our lower-bound calculation of 1.98 MPa $\sqrt{m}$. The overall agreement between our calculations and experimental values for TiC and TiN suggests that this method may work well for other technical ceramics and semiconductors.

Given the particularly brittle nature of Bi_2Te_3, the fracture toughness of polycrystalline samples can be $\sim$10$\times$ higher than the single crystal value due to crack blunting and deflection at grain boundaries. Particularly for highly anisotropic materials, grain orientation can be expected to play a significant role [51].

Additionally, it is important to note that many of the materials studied in this work were thermoelectric materials with very limited experimental data regarding fracture toughness. It must also be recognized that experimentally determining fracture toughness often introduces significant errors, particularly when calculated using the very common Vickers indentation method [79, 71]. Many of these measurements have an associated error upwards of 30% or more, and experimental details can greatly impact reported fracture toughness measurements[79, 80]. Thus, in comparing calculated fracture toughness values to experimental fracture toughness values, it should be kept in mind that both are aptly estimations, each with error associated. Relatively unreliable experimental methods like the Vickers indentation method are commonly used to characterize advanced brittle ceramics where more thorough experimental tests are impractical or expensive[54]. For these materials, the computational method outlined in this work can similarly provide an estimate of fracture toughness that does not require the laborious synthesis of large numbers of expensive materials.

Although the "ideal" strength of solids may not include defects [81], it is still possible to investigate the effects of defect structures on fracture toughness using this method [35, 33]. This is shown graphically in Supplemental Figure S22 where the stress-displacement curves for a defect-free Bi_2Te_3 crystal is compared with that of a nanotwinned structure[33]. In this case, the integral stress-displacement method revealed that nanotwinning improved fracture toughness by a factor of 2-4 relative to the defect free material. In general, computational techniques may provide a unique insight into the physics of fracture when point defects (e.g. vacancies or atomic substitutions), dislocations or defect structures (like grain boundaries) are included in the calculation. It has been shown experimentally [82, 83, 84] that the presence of defects can have varying degrees of impact on the fracture toughness depending on factors such as dislocation structure, grain boundary geometries, and defect pinning. The generality of the integral stress-displacement method lends itself to estimate fracture energies of various structures from the atomic to the microstructural scale, extending beyond the lower-limit estimation developed herein. Additionally, this method could be applied to 1D and 2D materials [44], as they also have an ideal strength. However only comparisons to bulk and thin film materials were made here.

Lastly, it should be noted that the estimates of fracture energy G found from slab calculations of surface energy and from the integral stress-displacement method were not always in agreement (Supplemental Note 2). The surface energy found by the slab method is for a relaxed structure and does not probe the continuous deformation of the material during fracture. Thus, while further investigation is needed to understand the discrepancy between the two methods, the integral stress-displacement method (Fig. 1) has been demonstrated to quantitatively agree with single crystal measurements, thereby providing a lower-limit value for technologically-relevant materials.

5 Conclusions

Ideal strength calculations can provide insights into fracture behavior at the atomic level. Using the proposed integral stress-displacement method, the fracture energies obtained from computational experiments of strain along weakest crystallographic directions gives an estimate for the lower-limit of fracture toughness. The results agree with single crystal experimental reports and provide a basis for more involved studies of fracture. The effects of defects like vacancies, interstitials, dislocations and grain boundaries may also be investigated within the framework of the integral stress-displacement method. Although fracture is inherently complicated, realistic values of fracture toughness can be calculated that can be used for computation based materials design [85], multiscale fracture models, or other engineering applications where benchmark or comparative values of fracture toughness are necessary. Since this work relies only on first principles, it could be used to anticipate the fracture toughness of new materials, allowing for bottom-up engineering towards the development of next-generation technologies.

6 Acknowledgements

MTA acknowledges support from the PPG graduate fellowship. MTA, JPM, and GJS acknowledge the support of award 70NANB19H005 from U.S. Department of Commerce, National Institute of Standards and Technology as part of the Center for Hierarchical Materials Design (CHiMaD). SA and GJS would like to acknowledge the National Science Foundation (NSF) DMREF award #1729487. SM was thankful for the support by Act 211 Government of the Russian Federation, under No. 02.A03.21.0011 and by the Supercomputer Simulation Laboratory of South Ural State University.

This material is based upon work supported by the National Science Foundation Graduate Research Fellowship Program under Grant No. DGE-1842165. Any opinions, findings, and conclusions or recommendations expressed in this material are those of the author(s) and do not necessarily reflect the views of the National Science Foundation.

Author contributions statement

MTA and GJS conceived the project. LB conducted the study. MTA and LB drafted the manuscript. GL and SIM performed DFT calculations. All authors contributed to the analysis and content of the manuscript.

Additional information

The authors declare no conflicts of interest, financial or otherwise.

References

1. S. Choi, E. Heller, D. Dorsey, R. Vetury, S. Graham, The impact of mechanical stress on the degradation of AlGaN/GaN high electron mobility transistors, Journal of Applied Physics 114 (16) (2013) 164501. doi:10.1063/1.4826524.
URL https://doi.org/10.1063/1.4826524

2. B. L. Hancock, M. Nazari, J. Anderson, E. Piner, F. Faili, S. Oh, D. Twitchen, S. Graham, M. Holtz, Ultraviolet micro-Raman spectroscopy stress mapping of a 75-mm GaN-on-diamond wafer, Applied Physics Letters 108 (21) (2016) 211901. doi:10.1063/1.4952596.
URL http://aip.scitation.org/doi/10.1063/1.4952596

3. Z. Zhang, Z. Yin, T. Han, A. C. Tan, Fracture analysis of wind turbine main shaft, Engineering Failure Analysis 34 (2013) 129–139. doi:10.1016/j.engfailanal.2013.07.014.
URL http://dx.doi.org/10.1016/j.engfailanal.2013.07.014

4. S. Park, C.-T. Sun, Fracture Criteria for Piezoelectric Ceramics, Journal of the American Ceramic Society 78 (6) (1995) 1475–1480. doi:10.1111/j.1151-2916.1995.tb08840.x.
URL http://doi.wiley.com/10.1111/j.1151-2916.1995.tb08840.x

5. D. R. Clarke, M. Oechsner, N. P. Padture, Thermal-barrier coatings for more efficient gas-turbine engines, MRS Bulletin 37 (10) (2012) 891–898. doi:10.1557/mrs.2012.232.
URL https://doi.org/10.1557/mrs.2012.232

6. J. Gubbi, R. Buyya, S. Marusic, M. Palaniswami, Internet of Things (IoT): A vision, architectural elements, and future directions, Future Generation Computer Systems 29 (7) (2013) 1645–1660. doi:https://doi.org/10.1016/j.future.2013.01.010.
URL http://www.sciencedirect.com/science/article/pii/S0167739X13000241

7. A. A. Griffith, The phenomena of rupture and flow in solids, Philosophical Transactions of the Royal Society of London. Series A, Containing Papers of a Mathematical or Physical Character 221 (1921) 163–198.
URL http://www.jstor.org/stable/91192

8. G. R. Irwin, Analysis of stresses and strains near the end of a crack traversing a plate, Trans. ASME, Ser. E, J. Appl. Mech. 24 (1957) 361–364.
URL https://imechanica.org/files/1957%20Irwin%20Analysis%20of%20stresses%20and%20strains%20near%20the%20end%20of%20a%20crack%20traversing%20a%20plate.pdf.

9. E. Orowan, Fracture and strength of solids, Reports on Progress in Physics 12 (1) (1949) 185–232. doi:10.1088/0034-4885/12/1/309.
URL https://iopscience.iop.org/article/10.1088/0034-4885/12/1/309

10. E. Orowan, Energy criteria of fracture, Welding Journal 34 (1955) 157–160.

11. J. R. Rice, Dislocation nucleation from a crack tip: An analysis based on the Peierls concept, Journal of the Mechanics and Physics of Solids 40 (2) (1992) 239–271. doi:10.1016/S0022-5096(05)80012-2.
URL https://www.sciencedirect.com/science/article/pii/S0022509605800122?via%3Dihub

12. G. T. Hahn, M. F. Kanninen, A. R. Rosenfield, Fracture Toughness of Materials, Annual Review of Materials Science 2 (1) (1972) 381–404. doi:10.1146/annurev.ms.02.080172.002121.
URL https://doi.org/10.1146/annurev.ms.02.080172.002121

13. W. M. Garrison, N. R. Moody, Ductile fracture, Journal of Physics and Chemistry of Solids 48 (11) (1987) 1035–1074. doi:https://doi.org/10.1016/0022-3697(87)90118-1.

URL http://www.sciencedirect.com/science/article/pii/0022369787901181

14. J. C. Boettger, J. R. Smith, U. Birkenheuer, N. Rösch, S. B. Trickey, J. R. Sabin, S. P. Apell, Extracting convergent surface formation energies from slab calculations, Journal of Physics: Condensed Matter 10 (4) (1998) 893–894. doi:10.1088/0953-8984/10/4/017.
URL https://doi.org/10.1088{%}2F0953-8984{%}2F10{%}2F4{%}2F017

15. V. Fiorentini, M. Methfessel, Extracting convergent surface energies from slab calculations, Journal of Physics: Condensed Matter 8 (36) (1996) 6525–6529. doi:10.1088/0953-8984/8/36/005.
URL https://doi.org/10.1088{%}2F0953-8984{%}2F8{%}2F36{%}2F005

16. P. A. Olsson, M. Mrovec, M. Kroon, First principles characterisation of brittle transgranular fracture of titanium hydrides, Acta Materialia 118 (2016) 362–373. doi:10.1016/j.actamat.2016.07.037.
URL https://doi.org/10.1016/j.actamat.2016.07.037

17. C. E. Dreyer, A. Janotti, C. G. Van De Walle, Brittle fracture toughnesses of GaN and AlN from first-principles surface-energy calculations, Applied Physics Letters 106 (21) (2015). doi:10.1063/1.4921855.
URL http://dx.doi.org/10.1063/1.4921855

18. J. Emmerlich, N. Thieme, M. To Baben, D. Music, J. M. Schneider, Stability, elastic properties and fracture toughness of Al 0.75X0.75B14 (X=Sc, Ti, V, Cr, Y, Zr, Nb, Mo) investigated using ab initio calculations, Journal of Physics Condensed Matter 25 (33) (2013). doi:10.1088/0953-8984/25/33/335501.
URL https://pubmed.ncbi.nlm.nih.gov/23877961/

19. P. A. Olsson, K. Kese, M. Kroon, A. M. Holston, Ab initio-based fracture toughness estimates and transgranular traction-separation modelling of zirconium hydrides, Modelling and Simulation in Materials Science and Engineering 23 (4) (2015) 45015. doi:10.1088/0965-0393/23/4/045015.
URL http://dx.doi.org/10.1088/0965-0393/23/4/045015

20. Z. Ding, S. Zhou, Y. Zhao, Hardness and fracture toughness of brittle materials: A density functional theory study, Physical Review B - Condensed Matter and Materials Physics 70 (18) (2004) 1–6. doi:10.1103/PhysRevB.70.184117.
URL https://link.aps.org/doi/10.1103/PhysRevB.70.184117

21. Y. W. Chung, Introduction to Materials Science and Engineering, CRC Press, 2007.

22. T. Ono, M. Ueki, Effect of Graphite Addition on the Microstructure and Mechanical Properties of Hot-pressed Titanium Carbide, 1994, pp. 585–588. doi:10.1016/B978-0-444-81991-8.50144-8.
URL http://www.sciencedirect.com/science/article/pii/B9780444819918501448

23. C. Maerky, M. O. Guillou, J. L. Henshall, R. M. Hooper, Indentation hardness and fracture toughness in single crystal TiC0.96, Materials Science and Engineering A 209 (1-2) (1996) 329–336. doi:10.1016/0921-5093(95)10152-7.
URL https://www.sciencedirect.com/science/article/abs/pii/0921509395101527

24. J. Buchinger, L. Löfler, J. Ast, A. Wagner, Z. Chen, J. Michler, Z. L. Zhang, P. H. Mayrhofer, D. Holec, M. Bartosik, Fracture properties of thin film TiN at elevated temperatures, Materials & Design 194 (2020) 108885. doi:https://doi.org/10.1016/j.matdes.2020.108885.
URL http://www.sciencedirect.com/science/article/pii/S0264127520304196

25. Y. Hu, J. H. Huang, J. M. Zuo, In situ characterization of fracture toughness and dynamics of nanocrystalline titanium nitride films, Journal of Materials Research 31 (3) (2016) 370–379. doi:10.1557/jmr.2016.4.
URL https://doi.org/10.1557/jmr.2016.4

26. D. L. Price, B. R. Cooper, J. M. Wills, Full-potential linear-muffin-tin-orbital study of brittle fracture in titanium carbide, Phys. Rev. B 46 (1992) 11368–11375. doi:10.1103/PhysRevB.46.11368.
URL https://link.aps.org/doi/10.1103/PhysRevB.46.11368

27. G. Kresse, J. Furthmüller, Efficiency of ab-initio total energy calculations for metals and semiconductors using a plane-wave basis set, Computational Materials Science 6 (1) (1996) 15–50. doi:10.1016/0927-0256(96)00008-0.
URL http://www.sciencedirect.com/science/article/pii/0927025696000080

28. G. Kresse, J. Furthmüller, Efficient iterative schemes for ab initio total-energy calculations using a plane-wave basis set, Phys. Rev. B 54 (1996) 11169–11186. doi:10.1103/PhysRevB.54.11169.
URL https://link.aps.org/doi/10.1103/PhysRevB.54.11169

29. G. Kresse, D. Joubert, From ultrasoft pseudopotentials to the projector augmented-wave method, Phys. Rev. B 59 (1999) 1758–1775. doi:10.1103/PhysRevB.59.1758.

URL https://link.aps.org/doi/10.1103/PhysRevB.59.1758

30. G. Li, Q. An, U. Aydemir, W. A. Goddard, M. Wood, P. Zhai, Q. Zhang, G. J. Snyder, Enhanced ideal strength of thermoelectric half-Heusler TiNiSn by sub-structure engineering, Journal of Materials Chemistry A 4 (38) (2016) 14625–14636. doi:10.1039/c6ta04123j.
URL https://pubs.rsc.org/en/content/articlelanding/2016/ta/c6ta04123j#!divAbstract

31. G. Li, U. Aydemir, B. Duan, M. T. Agne, H. Wang, M. Wood, Q. Zhang, P. Zhai, W. A. Goddard, G. J. Snyder, Micro- and Macromechanical Properties of Thermoelectric Lead Chalcogenides, ACS Applied Materials and Interfaces 9 (46) (2017) 40488–40496. doi:10.1021/acsami.7b15651.
URL https://doi.org/10.1021/acsami.7b15651

32. G. Li, U. Aydemir, M. Wood, W. A. Goddard, P. Zhai, Q. Zhang, G. J. Snyder, Ideal Strength and Deformation Mechanism in High-Efficiency Thermoelectric SnSe, Chemistry of Materials 29 (5) (2017) 2382–2389. doi:10.1021/acs.chemmater.7b00279.
URL https://pubs.acs.org/doi/10.1021/acs.chemmater.7b00279

33. G. Li, U. Aydemir, S. I. Morozov, M. Wood, Q. An, P. Zhai, Q. Zhang, W. A. Goddard, G. J. Snyder, Superstrengthening Bi2Te3 through Nanotwinning, Physical Review Letters 119 (8) (2017) 1–6. doi:10.1103/PhysRevLett.119.085501.
URL https://link.aps.org/doi/10.1103/PhysRevLett.119.085501

34. G. Li, Q. An, W. Li, W. A. Goddard, P. Zhai, Q. Zhang, G. J. Snyder, Brittle Failure Mechanism in Thermoelectric Skutterudite CoSb3, Chemistry of Materials 27 (18) (2015) 6329–6336. doi:10.1021/acs.chemmater.5b02268.
URL https://doi.org/10.1021/acs.chemmater.5b02268

35. G. Li, S. I. Morozov, Q. Zhang, Q. An, P. Zhai, G. J. Snyder, Enhanced Strength Through Nanotwinning in the Thermoelectric Semiconductor InSb, Physical Review Letters 119 (21) (2017) 1–6. doi:10.1103/PhysRevLett.119.215503.
URL https://link.aps.org/doi/10.1103/PhysRevLett.119.215503

36. G. Li, U. Aydemir, M. Wood, W. A. Goddard, P. Zhai, Q. Zhang, G. J. Snyder, Mechanical properties of thermoelectric lanthanum telluride from quantum mechanics, Journal of Physics D: Applied Physics 50 (27) (2017). doi:10.1088/1361-6463/aa7625.
URL https://iopscience.iop.org/article/10.1088/1361-6463/aa7625/meta

37. G. Li, U. Aydemir, M. Wood, Q. An, W. A. Goddard, P. Zhai, Q. Zhang, G. J. Snyder, Deformation mechanisms in high-efficiency thermoelectric layered Zintl compounds, Journal of Materials Chemistry A 5 (19) (2017) 9050–9059. doi:10.1039/c7ta02080e.
URL https://pubs.rsc.org/en/content/articlelanding/2017/ta/c7ta02080e#!divAbstract

38. D. Roundy, M. L. Cohen, Ideal strength of diamond, si, and ge, Phys. Rev. B 64 (2001) 212103. doi:10.1103/PhysRevB.64.212103.
URL https://link.aps.org/doi/10.1103/PhysRevB.64.212103

39. X. Li, S. Schönecker, J. Zhao, B. Johansson, L. Vitos, Ideal strength of random alloys from first principles, Physical Review B - Condensed Matter and Materials Physics 87 (21) (2013) 1–12. doi:10.1103/PhysRevB.87.214203.
URL https://journals.aps.org/prb/abstract/10.1103/PhysRevB.87.214203

40. C. R. Krenn, D. Roundy, J. W. Morris, M. L. Cohen, Ideal strengths of bcc metals, Materials Science and Engineering: A 319-321 (2001) 111–114. doi:https://doi.org/10.1016/S0921-5093(01)00998-4.
URL http://www.sciencedirect.com/science/article/pii/S0921509301009984

41. S. Ogata, J. Li, Y. Shibutani, S. Yip, Ab Initio Study of Ideal Shear Strength, 2004, pp. 401–410. doi:10.1007/978-1-4020-2111-4_38.
URL https://link.springer.com/chapter/10.1007%2F978-1-4020-2111-4_38

42. D. Roundy, C. R. Krenn, M. L. Cohen, J. W. Morris, The ideal strength of tungsten, Philosophical Magazine A: Physics of Condensed Matter, Structure, Defects and Mechanical Properties 81 (7) (2001) 1725–1747. doi:10.1080/01418610108216634.
URL https://doi.org/10.1080/01418610108216634

43. G. Li, Q. An, W. A. Goddard, R. Hanus, P. Zhai, Q. Zhang, G. J. Snyder, Atomistic explanation of brittle failure of thermoelectric skutterudite CoSb3, Acta Materialia 103 (2016) 775–780. doi:10.1016/j.actamat.2015.11.021.

44. B. Mortazavi, M. Silani, E. V. Podryabinkin, T. Rabczuk, X. Zhuang, A. V. Shapeev, First-principles multiscale modeling of mechanical properties in graphene/borophene heterostructures empowered by machine-learning interatomic potentials, Advanced Materials 33 (35) (2021) 2102807.

45. M. Černý, P. Šesták, P. Rehák, M. Všianská, M. Šob, Atomistic approaches to cleavage of interfaces, Modelling and Simulation in Materials Science and Engi-

neering 27 (3) (2019). doi:10.1088/1361-651X/ab0293.

46. M. Černý, J. Pokluda, On the effect of supercell size and strain localization in computational tensile tests, Modelling and Simulation in Materials Science and Engineering 28 (6) (2020) 65011. doi:10.1088/1361-651x/ab9f83.
URL https://doi.org/10.1088/1361-651x/ab9f83

47. C. Lamuta, A. Cupolillo, A. Politano, Z. S. Aliev, M. B. Babanly, E. V. Chulkov, L. Pagnotta, Indentation fracture toughness of single-crystal Bi2Te3topological insulators, Nano Research 9 (4) (2016) 1032–1042. doi:10.1007/s12274-016-0995-z.
URL https://link.springer.com/article/10.1007%2Fs12274-016-0995-z

48. F. Ericson, S. Johansson, J. Å. Schweitz, Hardness and fracture toughness of semiconducting materials studied by indentation and erosion techniques, Materials Science and Engineering 105-106 (PART 1) (1988) 131–141. doi:10.1016/0025-5416(88)90489-2.
URL http://www.sciencedirect.com/science/article/pii/0025541688904892

49. K. Yasutake, M. Iwata, K. Yoshii, M. Umeno, H. Kawabe, Crack healing and fracture strength of silicon crystals, Journal of Materials Science 21 (6) (1986) 2185–2192. doi:10.1007/BF00547968.
URL https://doi.org/10.1007/BF00547968

50. P. Gumbsch, J. Riedle, A. Hartmaier, H. F. Fischmeister, Controlling Factors for the Brittle-to-Ductile Transition in Tungsten Single Crystals, Science 282 (November) (1998) 1293–1295. doi:10.1126/science.282.5392.1293.
URL https://science.sciencemag.org/content/282/5392/1293

51. C. Ma, H. Liu, R. Chen, Q. Su, H. Cui, Y. Gu, Anisotropy thermoelectric and mechanical property of polycrystalline SnSe prepared under different processes, Journal of Materials Science: Materials in Electronics 30 (7) (2019) 6403–6410. doi:10.1007/s10854-019-00943-8.
URL https://doi.org/10.1007/s10854-019-00943-8

52. K. Tyagi, B. Gahtori, S. Bathula, N. K. Singh, S. Bishnoi, S. Auluck, A. K. Srivastava, A. Dhar, Electrical transport and mechanical properties of thermoelectric tin selenide, RSC Advances 6 (14) (2016) 11562–11569. doi:10.1039/c5ra23742d.
URL https://pubs.rsc.org/en/content/articlelanding/2016/ra/c5ra23742d#!divAbstract

53. R. Shu, Y. Zhou, Q. Wang, Z. Han, Y. Zhu, Y. Liu, Y. Chen, M. Gu, W. Xu, Y. Wang, W. Zhang, L. Huang, W. Liu, $Mg_{3+\delta}Sb_xBi_{2-x}$Family: A Promising Substitute for the State-of-the-Art n-Type Thermoelectric Materials near Room Temperature, Advanced Functional Materials 29 (4) (2019) 1807235. doi:10.1002/adfm.201807235.
URL http://doi.wiley.com/10.1002/adfm.201807235

54. J. M. Ma, S. A. Firdosy, R. B. Kaner, J. P. Fleurial, V. A. Ravi, Hardness and fracture toughness of thermoelectric La3-x Te 4, Journal of Materials Science 49 (3) (2014) 1150–1156. doi:10.1007/s10853-013-7794-7.
URL https://link.springer.com/article/10.1007%2Fs10853-013-7794-7#citeas

55. V. Ravi, S. Firdosy, T. Caillat, B. Lerch, A. Calamino, R. Pawlik, M. Nathal, A. Sechrist, J. Buchhalte, S. Nutt, Mechanical properties of thermoelectric skutterudites, in: AIP Conference Proceedings, Vol. 969, 2008, pp. 656–662. doi:10.1063/1.2845027.
URL https://aip.scitation.org/doi/pdf/10.1063/1.2845027

56. J. Eilertsen, M. A. Subramanian, J. J. Kruzic, Fracture toughness of Co4Sb12 and In 0.1Co4Sb12 thermoelectric skutterudites evaluated by three methods, Journal of Alloys and Compounds 552 (2013) 492–498. doi:10.1016/j.jallcom.2012.11.066.
URL https://www.sciencedirect.com/science/article/pii/S0925838812020506?via%3Dihub

57. W. Everhart, J. Newkirk, Mechanical properties of Heusler alloys, Heliyon 5 (5) (2019). doi:10.1016/j.heliyon.2019.e01578.
URL https://www.cell.com/heliyon/fulltext/S2405-8440(19)31885-7?_returnURL=https%3A%2F%2Flinkinghub.elsevier.com%2Fretrieve%2Fpii%2FS2405844019318857%3Fshowall%3Dtrue

58. R. R. Salem, J., E. Baker, Structural design parameters for germanium, Tech. Rep. 20160012342 (2017).
URL https://ntrs.nasa.gov/archive/nasa/casi.ntrs.nasa.gov/20160012342.pdf

59. B. Gludovatz, S. Wurster, A. Hoffmann, R. Pippan, Fracture toughness of polycrystalline tungsten alloys, International Journal of Refractory Metals and Hard Materials 28 (6) (2010) 674–678. doi:10.1016/j.ijrmhm.2010.04.007.
URL http://dx.doi.org/10.1016/j.ijrmhm.2010.04.007

60. R. W. Margevicius, J. Riedle, P. Gumbsch, Fracture toughness of polycrystalline tungsten under mode I and mixed mode I/II loading, Materials Science and Engineering A 270 (2) (1999) 197–209.

doi:10.1016/S0921-5093(99)00252-X.
URL https://www.sciencedirect.com/science/article/abs/pii/S092150939900252X

61. J. Fu, X. Su, H. Xie, Y. Yan, W. Liu, Y. You, X. Cheng, C. Uher, X. Tang, Understanding the combustion process for the synthesis of mechanically robust SnSe thermoelectrics, Nano Energy 44 (December 2017) (2018) 53–62. doi:10.1016/j.nanoen.2017.11.073.
URL https://doi.org/10.1016/j.nanoen.2017.11.073

62. X. Gao, J. Kim, Modeling of ductile fracture: Significance of void coalescence, International Journal of Solids and Structures 43 (20) (2006) 6277–6293. doi:https://doi.org/10.1016/j.ijsolstr.2005.08.008.
URL http://www.sciencedirect.com/science/article/pii/S0020768305005330

63. W. Li, P. Zhai, G. Li, X. Yang, L. Liu, Molecular dynamics simulation on mechanical properties of crystalline CoSb3 with nanopores, Materials Research Innovations 18 (sup4) (2014) S4–106–S4–109. doi:10.1179/1432891714Z.000000000656.
URL https://doi.org/10.1179/1432891714Z.000000000656

64. M. Sribalaji, B. Mukherjee, S. R. Bakshi, P. Arunkumar, K. Suresh Babu, A. K. Keshri, In-situ formed graphene nanoribbon induced toughening and thermal shock resistance of spark plasma sintered carbon nanotube reinforced titanium carbide composite, Composites Part B: Engineering 123 (2017) 227–240. doi:10.1016/j.compositesb.2017.05.035.
URL http://dx.doi.org/10.1016/j.compositesb.2017.05.035

65. I. T. Witting, T. C. Chasapis, F. Ricci, M. Peters, N. A. Heinz, G. Hautier, G. J. Snyder, The Thermoelectric Properties of Bismuth Telluride, Advanced Electronic Materials 5 (6) (2019) 1800904. doi:10.1002/aelm.201800904.
URL https://onlinelibrary.wiley.com/doi/abs/10.1002/aelm.201800904

66. T. D. Joseph, M. Tanaka, A. J. Wilkinson, S. G. Roberts, Brittle-ductile transitions in vanadium and iron-chromium, Journal of Nuclear Materials 367-370 A (SPEC. ISS.) (2007) 637–643. doi:10.1016/j.jnucmat.2007.03.077.
URL https://www.sciencedirect.com/science/article/abs/pii/S0022311507004916?via%3Dihub

67. F. Schwartzberg, H. Ogden, R. Jaffee, Ductile-Brittle Transition in Refractory Metals, Tech. rep., Defense Metals Information Center, Battelle Memorial Institute, Columbus, Ohio (1959).

68. J. Reiser, A. Hartmaier, Elucidating the dual role of grain boundaries as dislocation sources and obstacles and its impact on toughness and brittle-to-ductile transition, Scientific Reports 10 (1) (2020) 1–18. doi:10.1038/s41598-020-59405-5.
URL http://dx.doi.org/10.1038/s41598-020-59405-5

69. S. Liu, W. Hu, J. Xiang, F. Wen, B. Xu, D. Yu, J. He, Y. Tian, Z. Liu, Mechanical properties of nanocrystalline TiC–ZrC solid solutions fabricated by spark plasma sintering, Ceramics International 40 (7, Part B) (2014) 10517–10522. doi:https://doi.org/10.1016/j.ceramint.2014.03.024.
URL http://www.sciencedirect.com/science/article/pii/S0272884214003514

70. B. Mussler, M. V. Swain, N. Claussen, Dependence of Fracture Toughness of Alumina, Journal of the American Ceramic Society 65 (11) (1982) 566–572.

71. G. D. Quinn, R. C. Bradt, On the Vickers indentation fracture toughness test, Journal of the American Ceramic Society 90 (3) (2007) 673–680.

72. H. G. Leduc, B. Bumble, P. K. Day, B. H. Eom, J. Gao, S. Golwala, B. A. Mazin, S. McHugh, A. Merrill, D. C. Moore, et al., Titanium nitride films for ultrasensitive microresonator detectors, Applied Physics Letters 97 (10) (2010) 102509. doi:10.1063/1.3480420.
URL https://aip.scitation.org/doi/abs/10.1063/1.3480420?journalCode=apl

73. A. Achour, R. L. Porto, M.-A. Soussou, M. Islam, M. Boujtita, K. A. Aissa, L. Le Brizoual, A. Djouadi, T. Brousse, Titanium nitride films for micro-supercapacitors: effect of surface chemistry and film morphology on the capacitance, Journal of Power Sources 300 (2015) 525–532. doi:10.1016/j.jpowsour.2015.09.012.
URL http://www.sciencedirect.com/science/article/pii/S0378775315302731

74. L. Gui, S. Bagheri, N. Strohfeldt, M. Hentschel, C. M. Zgrabik, B. Metzger, H. Linnenbank, E. L. Hu, H. Giessen, Nonlinear refractory plasmonics with titanium nitride nanoantennas, Nano letters 16 (9) (2016) 5708–5713. doi:10.1021/acs.nanolett.6b02376.
URL https://pubs.acs.org/doi/abs/10.1021/acs.nanolett.6b02376

75. E. Santecchia, A. Hamouda, F. Musharavati, E. Zalnezhad, M. Cabibbo, S. Spigarelli, Wear resistance investigation of titanium nitride-based coatings, Ceramics International 41 (9) (2015) 10349–10379. doi:10.1016/j.ceramint.2015.04.152.
URL http://www.sciencedirect.com/science/article/pii/S0272884215009116

76. P. Chen, W.-Y. Wu, The use of sputter deposited tin thin film as a surface conducting layer on the counter electrode of flexible plastic dye-sensitized solar cells, Surface and Coatings Technology 231 (2013) 140–143. doi:10.1016/j.surfcoat.2012.06.054.
URL https://www.sciencedirect.com/science/article/abs/pii/S0257897212006238

77. B. G. Kim, C. Jo, J. Shin, Y. Mun, J. Lee, J. W. Choi, Ordered mesoporous titanium nitride as a promising carbon-free cathode for aprotic lithium-oxygen batteries, ACS nano 11 (2) (2017) 1736–1746. doi:10.1021/acsnano.6b07635.
URL https://pubs.acs.org/doi/10.1021/acsnano.6b07635

78. B. Avasarala, P. Haldar, Durability and degradation mechanism of titanium nitride based electrocatalysts for pem (proton exchange membrane) fuel cell applications, Energy 57 (2013) 545–553. doi:10.1016/j.energy.2013.05.021.
URL https://www.sciencedirect.com/science/article/abs/pii/S0360544213004052

79. F. Sergejev, M. Antonov, Comparative study on indentation fracture toughness measurements of cermets and hardmetals, Euro PM 2006 - Powder Metallurgy Congress and Exhibition 1 (2006) 43–48.

80. A. Moradkhani, H. Baharvandi, M. Tajdari, H. Latifi, J. Martikainen, Determination of fracture toughness using the area of micro-crack tracks left in brittle materials by Vickers indentation test, Journal of Advanced Ceramics 2 (1) (2013) 87–102. doi:10.1007/s40145-013-0047-z.

81. A. Kelly, N. H. Macmillan, Strong solids, 3rd Edition, Monographs on the physics and chemistry of materials, Clarendon Press, Oxford, 1986.

82. Z. Jiuxing, L. Lu, Z. Meiling, H. Yancao, Z. Tieyong, Fracture toughness of sintered Mo-La2O3 alloy and the toughening mechanism, International Journal of Refractory Metals and Hard Materials 17 (6) (1999) 405–409. doi:10.1016/S0263-4368(99)00030-X.
URL https://www.sciencedirect.com/science/article/abs/pii/S026343689900030X?via%3Dihub

83. M. Danylenko, Y. Podrezov, S. Firstov, Effect of dislocation structure on fracture toughness of strained BCC-metals, Theoretical and Applied Fracture Mechanics 32 (1) (1999) 9–14. doi:10.1016/S0167-8442(99)00021-X.
URL https://www.sciencedirect.com/science/article/abs/pii/S016784429900021X?via%3Dihub

84. A. A. Kaminskiĭ, M. S. Akchurin, R. V. Gaĭnutdinov, K. Takaichi, A. Shirakava, H. Yagi, T. Yanagitani, K. Ueda, Microhardness and fracture toughness of Y2O3- and Y3Al5O12-based nanocrystalline laser ceramics, Crystallography Reports 50 (5) (2005) 869–873. doi:10.1134/1.2049410.
URL https://link.springer.com/article/10.1134%2F1.2049410

85. W. Xiong, G. B. Olson, Integrated computational materials design for high-performance alloys, MRS Bulletin 40 (12) (2015) 1035–1043. doi:10.1557/mrs.2015.273.
URL https://www.cambridge.org/core/journals/mrs-bulletin/article/integrated-computational-materials-design-for-h1C8766847E85BDFE152C158D7C7A4600